Journal of Environmental Management 349 (2024) 119461

Contents lists available at ScienceDirect

Journal of Environmental Management

journal homepage: www.elsevier.com/locate/jenvman

Research article

LED-driven photo-Fenton process for micropollutant removal by nanostructured magnetite anchored in mesoporous silica

J. González-Rodríguez [a,*], J.J. Conde [a], Z. Vargas-Osorio [b,c], C. Vázquez-Vázquez [c], Y. Piñeiro [c], J. Rivas [c], G. Feijoo [a], M.T. Moreira [a]

[a] CRETUS, Department of Chemical Engineering, Universidade de Santiago de Compostela, 15782, Santiago de Compostela, Spain
[b] Department of Biomaterials, Centre for Functional and Surface Functionalized Glass (FUNGLASS), Alexander Dubcek University of Trencin, Slovakia
[c] Laboratory of Magnetism and Nanotechnology, Department of Physical Chemistry, Faculty of Chemistry, and Applied Physics, Universidade de Santiago de Compostela, 15782, Santiago de Compostela, Spain

ARTICLE INFO

Handling Editor: Prof Raf Dewil

Keywords:
Reusability
Degradation pathways
Kinetics
Magnetic nanoparticles
LED
Supported catalysts

ABSTRACT

The presence of organic micropollutants in water bodies represents a threat to living organisms and ecosystems due to their toxicological effects and recalcitrance in conventional wastewater treatments. In this context, the application of heterogeneous photo-Fenton based on magnetite nanoparticles supported on mesoporous silica (SBA15) is proposed to carry out the non-specific degradation of the model compounds ibuprofen, carbamazepine, hormones, bisphenol A and the dye ProcionRed®. The operating conditions (i.e., pH, catalyst load and hydrogen peroxide concentration) were optimized by Response Surface Methodology (RSM). The paramagnetic properties of the nanocatalysts allowed their repeated use in sequential batch operations with catalyst losses below 1%. The feasibility of the process was demonstrated as removal rates above 90% after twelve accomplished after twelve consecutive cycles. In addition, the contributions of different reactive oxygen species, mainly $^{\bullet}$OH, were analyzed together with the formation of by-products, achieving total mineralization values of 15% on average.

CRediT author statement

Jorge González-Rodríguez: conceptualization, investigation, writing – original draft preparation, writing – review and editing Julio J. Conde: writing – review and editing and conceptualization Zulema Vargas-Osorio, Yolanda Piñeiro and Jose Rivas: resources Carlos Vázquez-Vázquez: writing – review and editing, conceptualization and supervision Gumersindo Feijoo: conceptualization and supervision Maria-Teresa Moreira: writing–review and editing, conceptualization and supervision. All authors have read and agreed to the published version of the manuscript.

1. Introduction

Scientific advances occurred since the industrial revolution have led to the development of new, more active, complex, and recalcitrant organic molecules, leading to the generation of more polluted wastewaters (Gavrilescu et al., 2015; Lu et al., 2015). In this regard, the changes in consumption patterns and the exponential population growth led to the increasing presence of micropollutants associated with anthropogenic activities in wastewater treatment plants (WWTPs) (Proctor et al., 2021). The chemical complexity and recalcitrant nature of most of these organic micropollutants commonly hinder their removal by the conventional treatments (Pai et al., 2020). Consequently, the physical and biological treatments become inefficient facing the reduction of these pollutants prior to the discharge of treated water (Couto et al., 2019; Craddock et al., 2020; Martínez-Alcalá et al., 2020).

Accordingly, the development of innovative wastewater treatment technologies is in line with 3rd and 6th Sustainable Development Goals (SDGs). In this regard, the application of innovative wastewater treatments ensures healthy ecosystems and the well-being of society by improving water. In addition, innovative research related to the improvement of sustainable water management partially meets the 13th SDG on combating climate change (United Nations, 2015). These changes are affecting water quality and availability, as the hydrological cycle is closely linked to climate behavior (DeNicola et al., 2015). However, the issue of water scarcity is not only related to water supply in quantity, but also to water quality, as the use of water sources with

* Corresponding author.
E-mail address: jorgegonzalez.rodriguez@usc.es (J. González-Rodríguez).

https://doi.org/10.1016/j.jenvman.2023.119461
Received 20 July 2023; Received in revised form 20 October 2023; Accepted 21 October 2023

high percentages of reused water may contain micropollutants (Müller et al., 2020).

In this sense, advanced oxidation processes (AOPs) could degrade a wide range of pollutants through the generation of reactive oxygen species (ROS), representing a feasible alternative for treating polluted effluents (Tufail et al., 2020). The high removal efficiencies achieved by these processes make possible their application in multiple fields of wastewater treatment. For instance, domestic and different types of industrial effluents with high pollutant load are candidates for their application (Lv et al., 2020). The most widely applied AOP in wastewater treatment is ultraviolet (UV) photolysis mainly due to its simplicity and minimal operational costs. Although this technique it is effective for pathogen removal, it is reported to be ineffective for the abatement of recalcitrant organic molecules (de Boer et al., 2022). Other AOPs such as semiconductor photocatalysis, anodic oxidation, ozonation or Fenton-based processes are being investigated by several authors for their application as tertiary treatments with the aim of improving the removal of these compounds (Tufail et al., 2020). Accordingly, the use of nanostructured catalysts in Fenton-based processes provides numerous advantages such as negligible sludge generation, improved recyclability of iron species and efficient production of hydroxyl radicals (Pisharody et al., 2022). One of the nanomaterials advantages is related to the increase of contact surface between target compounds and catalyst, which enhances the reaction rates (Sadegh et al., 2021). At these types of heterogeneous reactions, magnetite acts as an iron supplier for the catalytic decomposition of hydrogen peroxide. These reactions follow the same mechanistic pathways as reported by homogeneous Fenton (Minella et al., 2014). Furthermore, conventional Fenton processes are amenable to be improved by incorporating light sources promoting new reaction pathways to regenerate Fe-based catalysts (Mirzaei et al., 2017). In addition, the use of supported magnetite nanoparticles with superparamagnetic properties allows the recovery of materials in subsequent cycles (González-Rodríguez et al., 2021).

In this work, the nanocomposite Fe_3O_4@PAA/SBA15, a polyacrylic acid-coated and inert silica-supported magnetite, was studied to increase its reusability and degradation efficiency in photo-Fenton micropollutant abatement reactions. The effectivity of the treatment was tested using three hormones (estrone, estradiol and 17α-ethinylestradiol), a personal care product (bisphenol A) and an inflammatory drug (carbamazepine) as target compounds. The superparamagnetic properties of the nanostructured magnetite allow the separation of the effluent by applying an external magnetic field, which represents an important advantage for the industrial application. Moreover, the use of an energy-efficient light source aims to reduce energy consumption compared to conventional UV irradiation. The influence of the most important parameters for full-scale application - i.e., pH, catalyst concentration and hydrogen peroxide loading - was investigated, using a real wastewater matrix. In addition, complementary studies as the contribution of ROS species and the formation of transformation products were made to further investigate the mechanistic aspects of LED-driven photo-Fenton catalysis. The novelty of this work encompasses the use of a treatment technology with low energetic requirements compared to photocatalytic UV-based processes. It has been achieved removal percentages higher than 90% on the degradation of priority pollutants in real wastewater matrices, analyzing the degradation mechanisms of three endocrine disrupting chemicals.

2. Materials and methods

2.1. Catalyst synthesis

A magnetite-based catalyst supported on a SBA15 (Fe_3O_4@PAA/SBA15) matrix was used for the removal of different pollutants by the heterogeneous photo-Fenton method. The synthesis of SBA15 matrix was made following the method proposed by Colilla et al. (2007), using a Pluronic P123 (PEO_{20}-PPO_{70}-PEO_{20}) triblock polymer. For the synthesis of magnetite-based nanocomposites, the method proposed initially by Massart (1981) was applied with some modifications. At this modified procedure, the presence of SBA15 matrix in the reaction medium promotes the immobilization of magnetite on the surface of this type of mesoporous silica (Vargas-Osorio et al., 2017).

The synthesis procedure of magnetic nanocomposites starts with the incubation of SBA15 matrix, previously synthesized, together with a mixture of iron species containing Fe^{3+} and Fe^{2+} (molar ratio of 1.5) (González-Rodríguez et al., 2021). These salts are incubated for 30 min to promote adsorption of the iron ions on the matrix surface. Then, the formation of magnetite nanoparticles was favored by the addition of NH_4OH, that promotes the precipitation of ions over the SBA15 matrix. Once the precipitation of black magnetite occurs caused by the shifting of pH to an alkaline value, the as-formed composites are incubated for 1 h. At the end of this step, polyacrylic acid was added NH_4OH generating electrostatic repulsive interactions between magnetite and thus protecting the photocatalyst facing to agglomeration. Finally, the synthesized nanoparticles with magnetic properties are separated from the final solution by applying an external magnetic field. The catalyst is washed several times with distilled water to remove the organic residues of the synthesis.

The use of a triblock copolymer (Pluronic P123) for the synthesis of SBA15 enables the creation of large pore diameters and thick walls, thus producing a very stable material (Deng et al., 2013). The hexagonal structure of the mesoporous silica matrix allows the deposition of magnetite nanoparticles forming small aggregates distributed along its surface. In addition, the synthesis procedure through the coprecipitation of iron salts leads to the formation of nanoparticles even within the mesoporous silica channels. The size of the mesoporous matrix is in the micrometer range, which is much larger compared to the rest of the nanoparticles considered, which have sizes ranging from 5 to 20 nm. Furthermore, the zeta potential of the nanoparticles, essential to predict the stability of the nanoparticles and the interactions between the materials and the target compounds, showed negative values at pH 3. For a detailed characterization of these nanoparticles, see González-Rodríguez et al. (2021).

2.2. Photodegradation experiments

The degradation experiments were performed under a commercial LED lamp (20 W, 6000 K) purchased from Mas Lighting® LED (Lugo, ES). The lamp was used to irradiate twelve borosilicate reactors under magnetic stirring. Each reactor had a volume of 10 mL, with a variable catalyst concentration between 25 and 250 mg L^{-1}, hydrogen peroxide ranging from 25 to 350 mg L^{-1} and pH from 3 to 7. The matrix used for the first step of the experiments was distilled water, to avoid interferences caused by salts, dissolved compounds, or suspended solids. Once the optimal conditions were reached, the reaction was developed in a treated effluent of a secondary clarifier. The concentration of contaminants was monitored during the experiments by taking 250 μL aliquots, which were centrifuged at 6000 rpm for 3 min to ensure the removal of the nanoparticles. In addition, three replicates of all experiments were performed to minimize experimental errors and to quantify the standard deviation of the results.

The initial concentration of the target compound was set at 20 mg L^{-1} for the ProcionRed® and 300 μg L^{-1} for each of the pharmaceuticals (E1, E2, EE2, BPA, and CBZ). Quantification of the ProcionRed® dye was conducted by UV–Vis spectrophotometry on a PowerWave XS2 (BioTek, Winnoski, VT, US), measuring the concentration at the point of maximum absorbance (538 nm). The concentration of the pharmaceuticals was measured using an X-LC™ Jasco (Hachioji, 13, JP) high-performance liquid chromatography equipped with a diode array detector (HPLC-DAD) and a C_{18} Gemini® chromatographic column (3 μm, 110 Å, 4.6 × 150 mm). For elution, a 55:45 ACN:H_2O solution was used, at 35 °C and a flow rate of 0.8 mL min^{-1}. The determination of concentration was performed for each compound from eight duplicates

obtaining a regression coefficient (R^2) higher than 0.99.

The transformation compounds were determined in a TimsTOF Pro 2 UHPLC OLE-ELUTE (Brucker, Billerica, MA, US) equipped with atmospheric pressure chemical ionization (APCI), Tims-QTOF analyzer and on-line extraction system (OLE). The UHPLC is equipped with an Intensity Solo C18 column (2 μm, 90 Å, 2.1 × 100 mm) from Brucker and the acquisition range for samples was 50–1000 m/z. The injection volume was 100 μL and the solvents used for the extraction were water and acetonitrile. A mobile phase composed by H_2O_2/FA and MeOH was used for the elution of samples, based on the method reported by Vanderford et al. (2003). Aliquots of degradation experiments were taken after 15, 30 and 60 min and measured without pretreatment. Moreover, blank experiments without the target estrogens were conducted to quantify the matrix effects. The procedures followed for wastewater characterization, kinetic calculations and single contribution of reactive oxygen species (ROS) can be found in Supplementary Material.

2.3. Statistical optimization

The influence of the experimental conditions over the kinetics was studied by monitoring the degradation of the target compound ProcionRed®. For this purpose, was applied a fractional factorial experiment at three levels, analyzing the results using the Response Surface Methodology (RSM). Catalyst dosage between 25 and 250 mg L^{-1}, hydrogen peroxide concentration 25 and 350 mg L^{-1}, and pH from 3 to 7 were selected as the most important independent parameters. Their influence on the photo-Fenton process was studied analyzing the reaction rate constant as the dependent variable.

The calculation of kinetic constants was performed using three replicate data sets taking five aliquots between 0 and 90 min. Although there are multiple variables that can influence the reaction kinetics, wastewater composition or influent pollutant load cannot be easily controlled for an optimization study. Additionally, focusing on the application of this process for wastewater treatment plants, the temperature of the influent was also disregarded.

As the degradation kinetics follow a pseudo-first order model, the initial pollutant concentration was not considered for this analysis, as the reaction rate is independent of the initial dye concentration. Data processing and ANOVA calculations were done using StatGraphics software. Moreover, several control experiments (i.e., degradation due to hydrogen peroxide, absorption, photolysis, stability in reaction medium) were performed to analyze the single contribution on degradation rates.

3. Results and discussion

3.1. Optimization of reaction conditions

3.1.1. Response surface methodology for parameter optimization

As reported in previously Section 2.5, the RSM is a statistical tool to analyze the effect on a response variable due to the modification of certain inputs. At this case, the hydrogen peroxide concentration, the pH, and catalyst concentration were selected as critical operation variables. The optimum pH for homogeneous Fenton reaction is around 2.8–3.0, due to the higher oxidation potentials of generated radicals at acidic conditions as well as the high reaction rates. However, the natural pH of wastewaters is near to neutral, in a typical range between 5.5 and 8.0. From the operational point of view, the avoiding of pH shift in a conditioning step after and before the reaction represents a clear advantage on the application of this technology. Thus, the selected lower limit of pH at this study was 3 and the upper limit was 7.

In the same way, considering the reusability of catalyst after the photocatalytic reaction applying an external magnetic field, the concentration of magnetite does not imply the reagent consumption. The typical concentration for heterogeneous catalysts ranges from 0.1 to 1.0 g L^{-1}, however, a high concentration may suppose the shielding of light in the solution. At this study, an interval between 25 and 250 mg L^{-1} was selected. Finally, the hydrogen peroxide concentration typically is studied in the range 10–100 mg L^{-1}, although at this study the interval was extended to 25–350 mg L^{-1} (de Boer et al., 2022).

Once the RSM was performed under these limits, further experiments were conducted to obtain the optimum point, the full results of which are shown in Tables S2–S4 and summarized in Table S5. The results were fitted to a pseudo-first order kinetic model, showing an adequate fit with mean values of all calculated R^2 of 0.971 ± 0.019. According to the analysis of variance (ANOVA) results and considering that the R^2 value was 0.962 (adjusted R^2 = 0.956), the model accurately represents the behavior of the system. Furthermore, the use of the kinetic constant values instead of the removal of the target pollutant for a selected time provides additional robustness to the model, as each data point was calculated using values from six aliquot samples. Statistical analysis shows that eight effects have a p-value of less than 0.05, indicating a 95% confidence level that the effects are significant. The only effect found to be non-significant for degradation kinetics was the interaction between the catalyst and hydrogen peroxide concentrations.

In agreement with the results obtained, the most influential parameter in photo-Fenton catalysis was pH, according to the linear and quadratic values attained in their model. In addition, the parameter ranking second was the catalyst concentration, as reported by Grassi et al. (2020), which follows a linear response, while it shows a quadratic term in Saeed et al. (2021). Both papers analyzed the kinetic parameters using response surface methodology for dye removal using heterogeneous iron-based catalysts. The least influential parameters for all cases were the mixed interactions between the catalyst and the other parameters.

Furthermore, control experiments (data not shown) performed to discern between the actual contribution of photocatalysis and degradation by other parameters (light irradiation, addition of hydrogen peroxide and the combination of light and hydrogen peroxide) indicated that the influence of photolysis was negligible compared to photocatalysis. These results agree with those reported by Gultekin and Ince (2004) on the degradation of different types of dyes using advanced oxidation processes based on light irradiation.

3.1.2. Effect of operating parameters on ProcionRed® removal

The most influential factor for the degradation kinetics was the pH of the matrix, leading to highly significant linear and quadratic factors. The predominant influence of pH compared to other parameters, such as catalyst and hydrogen peroxide concentrations, was observed by other authors for Fenton-based processes (Abd Manan et al., 2019; Donadelli et al., 2020). In all cases, lower pH values contribute significantly to a faster degradation of the target compounds. Increasing the pH above neutral values results in a higher rate of decomposition of hydrogen peroxide into water and oxygen, whereby the occurrence of this decomposition leads to inefficient dosing of the bulk oxidant increasing treatment costs (Lyngsie et al., 2018; Smith and Nicoll, 1955). Moreover, the influence of pH on photocatalytic system may be attributed to the higher redox potential of ·OH radicals in acidic medium (2.80 V) compared to the potential in basic medium (1.89 V) (Sharma, 2012). In the case of hydrogen peroxide, the redox potential decays from 1.78 V to 0.88 V when reacting in basic medium (Feng et al., 2018).

Moreover, the combined effect of pH and hydrogen peroxide concentration as well as the combination of pH with catalyst concentration were significant. Their negative values mean that an increase in pH value must be followed by a reduction in catalyst and/or hydrogen peroxide concentration to fight against the decrease on kinetics. The response surface and contour lines at a fixed pH of 3 are shown in Fig. 1. At this graph is observed a maximum value for reaction rate, as well as the influence of H_2O_2 and nanoparticle concentration. Considering the maximum value represented by a cross in the Figure, the reduction of hydrogen peroxide only produces a decrease of 15% in reaction rate, since the catalyst change causes a decrease of a 22%. However, the

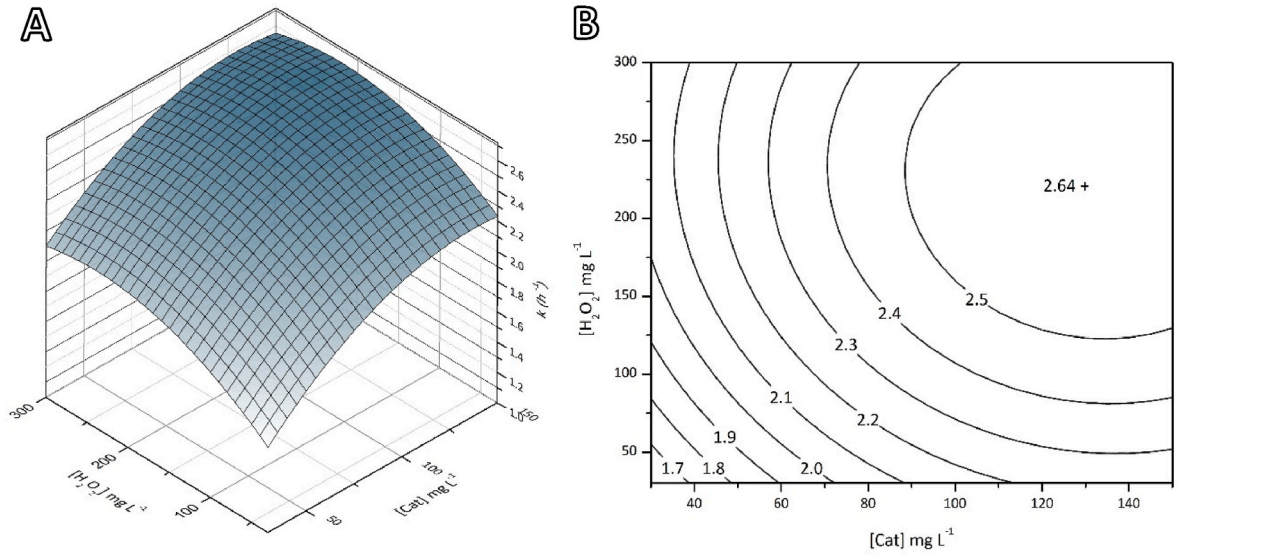

Fig. 1. (A) Response surface at pH 3 and (B) contour lines and optimum point of reaction rate for the removal of ProcionRed® (kinetic constant values are in h^{-1}).

combined effect only is responsible for the 35% of maximum value also showing the high influence of pH. For a complete summary of the results, please refer to Fig. S1 in the Supplementary material.

The Pareto diagram, depicted in Fig. 2, shows the influence of the distinct factors analyzed. In the case of catalyst concentration, the positive influence of the first-order factor and the negative value of the second-order interaction indicate that a high catalyst concentration contributes to a higher degradation. However, when the concentration reaches the upper experimental limits, kinetics are affected due to hindering of light in the colloidal suspension. The presence of suspended solids in a liquid-solid biphasic system causes turbidity, limiting the access of light to the overall reaction volume. Therefore, the presence of liquid fractions with a poor irradiation causes the decrease on reaction rates. Normally this limitation is overcome through reactor design, i.e., ensuring the reduction of cross section subjected to irradiation in photocatalytic reactors.

These results were in alignment with other studies, such as Nadeem et al. (2022), in which the influence of catalyst and oxidant concentration were analyzed, as well as the impact of dye concentration on the degradation rate of methylene blue. Although pH was studied independently of the RSM methodology, the results indicated that pH values between 3 and 7 provided the best degradation values. Furthermore, the most relevant factors were the oxidant and catalyst concentrations, with the dye concentration being the least significant parameter. The negative effect of high concentrations of hydrogen peroxide was explained by Gultekin and Ince (2004), because it acts as an auto-scavenger, hindering radical generation and consequently reducing the reaction rate. Thus, the reaction between the previously generated hydroxyl radicals with hydrogen peroxide present in the reaction matrix led to a decrease in reaction rates.

Comparing the results of this work with the obtained using other types of irradiations as UV or fluorescent tubes, the influence of pH at this system is most remarkable compared to catalyst and hydrogen peroxide concentration (González-Rodríguez et al., 2021). Moreover, the use of LED light enables the flexibilization of requirements in terms of hydrogen peroxide concentration. This lower influence allows a reduction on oxidant concentration, thus minimizing the reagent consumption.

3.1.3. Optimum point verification

The optimum point to maximize the micropollutant degradation can be obtained mathematically using the model equation. These conditions are pH 3.0, a catalyst concentration of 131 mg L^{-1} and a hydrogen peroxide concentration of 223 mg L^{-1}. The theoretical value of k under these conditions is 2.640 ± 0.172 h^{-1}, equivalent to a half-life of 15.75 ± 1.02 min^{-1}. As RSM is a statistical method that provides an optimal

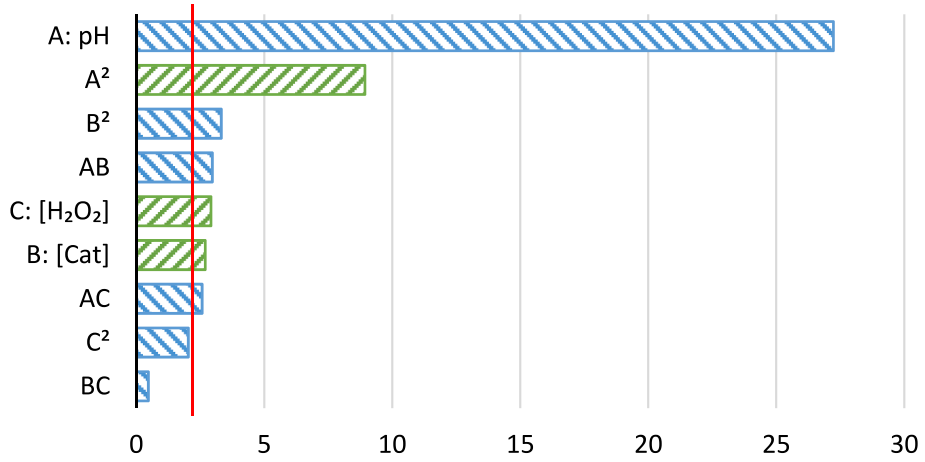

Fig. 2. Pareto chart for RSM optimization: positive effects (green bars), negative effects (blue bars) and level of significance for $p < 0.05$ (red line)

value by interpolation of real values, these conditions were assessed to compare the theoretical result with the experimental results. The kinetic constant obtained by applying the optimal parameters was 2.461 ± 0.114 h^{-1} and is statistically equal to the estimated value (2.640 ± 0.172 h^{-1}) considering a confidence level of $p < 0.05$.

Additionally, Fig. S2 represents a real experiment using the (a) optimum point provided by the RSM methodology, together with two experiments performed at pH 3 in which (b) the catalyst and hydrogen peroxide concentration is fixed at 50 and 150 mg L^{-1} and (c) using a catalyst and hydrogen peroxide concentration of 100 and 200 mg L^{-1}, respectively. These values were compared to determine the predictability of the method.

The degradation efficiency of the studied nanocomposite present similar optimum values and kinetic constants in comparison with other published heterogeneous photocatalysis studies for dye degradation. Xiang et al. (2020) reported similar optimum conditions using Fe-based nanoparticles, analyzing the removal of methyl orange in a photo-Fenton system. Rambu et al. (2018) studied the removal of azo dyes reaching degradation values for Reactive Yellow 84 higher than 80% after 120 min of reaction, using magnetite nanoparticles coated with polyethylene glycol and ferrous oxalate. However, the catalyst stability analysis showed a significant decay when the nanoparticles were reused. Kokate et al. (2022) used photocatalytic activation of peroxymonosulfate by LED irradiation and, by testing the degradation rate with an initial concentration of 10 mg L^{-1}, a kinetic constant of 5.64 h^{-1} for the azo dye Acid Orange 7 using g-C_3N_4-based catalyst was achieved.

In the specific case of Procion Red®, some works such as So et al. (2002) provided similar heterogeneous reaction rates under the optimal operating conditions. These authors reached a pseudo-first kinetic constant of 3 h^{-1} using TiO_2 with a concentration of 500 mg L^{-1}. Despite the similarity of both processes in terms of degradation time, the proposed process using magnetically recoverable catalyst provides an advantage from an operational point of view. Compared to homogeneous Fenton, the degradation kinetic constants of Procion Red® were lower, mainly due to mass transfer limitations. However, the main benefit of the heterogeneous process is that free iron is not detected in the effluent (Rodrigues et al., 2009).

3.1.4. Electric energy per order calculation

The electrical energy per order was calculated for the optimized experimental conditions, following Eq. (4). The obtained value was 67.72 kWh m^{-3} $order^{-1}$, considering that the lamp energy has been used to irradiate twelve samples at a time. This value is similar compared to the obtained by other authors under LED irradiation. For example, Kokate et al. (2022) obtained a value of 24.51 kWh m^{-3} $order^{-1}$ for the degradation of Acid Orange 7, but using a non-magnetic catalyst, while Ferreira et al. (2021) reported an E_{Eo} of 48.7 kWh m^{-3} $order^{-1}$ using homogeneous Fenton at pH 3 and under UV-A LED irradiation.

These nanoparticles have been used for the degradation of Acid Orange 7 and sulfamethoxazole using a UV irradiation, achieving a E_{Eo} of 274.0 and 965.8 kWh m^{-3} $order^{-1}$. When the UV light was replaced by fluorescent tubes, the values decayed to a half of their initial value (González-Rodríguez et al., 2021). Thus, the substitution of light sources for others more efficient in electrical consumption supposes a great advance on this technology.

$$E_{Eo} = \frac{P \cdot t}{60 \cdot V \cdot \ln\left(\frac{C_i}{C_f}\right)} = \frac{P}{V \cdot k} \quad (4)$$

3.2. Influence of radical species

Radicals play an essential role in photocatalytic degradation of organic molecules; hence, the influence of radical species was analyzed to quantify the individual contribution of each type of radical to the overall reaction rate. The results of the scavenging effects are shown in Fig. 3, while for the experimental details of scavenger experiments, please check the specific section and Table S6 in the Supplementary material.

The addition of ascorbic acid resulted in a kinetic constant reduction from 2.461 to 2.137 h^{-1}, which corresponds to a decrease of 13%, indicating that the contribution of adsorbed $^{\bullet}OH$ and $O_2^{\bullet-}$ radicals is not significant on the overall reaction rate. However, the free radical quenching assay using aliphatic alcohols suggests that the major contribution is due to the free hydroxyl radical generation. In these tests, the reaction rate decreased by 82% for both the MeOH and i-PrOH experiments. The formation of these hydroxyl radicals is a consequence of the decomposition of hydrogen peroxide in the presence of light and iron. The relative abundance of this radical was reported by other authors as the main contribution to the overall reaction using iron-based catalysts (Da Cruz Severo et al., 2020; Hernández-Oloño et al., 2021).

Different authors also reported the remarkable role of the combined $^{\bullet}OH$, $O_2^{\bullet-}$ and $^1O_2$ radicals in the Fenton-type process, as well as the predominant role of the hydroxyl radical in the reaction kinetics. This high contribution of $^{\bullet}OH$ caused the generation of by-products and partial mineralization of compounds through the generation of hydroxylated transformation products, as seen in Section 3.5. However, with respect to the results, the role of the superoxide radical and singlet oxygen in this process is less than that reported for other reactive systems (Ahmed et al., 2022; Liu et al., 2022).

Hydroxyl radicals attack organic pollutants through four basic pathways, as reported by Deng et al. (2015): radical addition, electron transfer, hydrogen abstraction, and radical combination. This attack produces carbon centered radicals, that in combination with oxygen lead to the degradation of chemicals by their partial mineralization. This ring opening through the addition of hydroxyl groups may be viewed in transformation product TP-276 in Section 3.5, as well as the reduction on molecular weight caused by the reactions with radicals (e.g., TP-160). On the other hand, the formation of hydroxylated parent compounds as TP-290 represents an intermediate step after the carbon loss.

3.3. Evaluation of the removal of emerging contaminants and pathogens

Once the influence of the reaction parameters was evaluated, optimal conditions were selected to perform the micropollutant degradation experiments in a real wastewater matrix. The micropollutants were selected considering their presence in the wastewater and their recalcitrant properties. Following these criteria, carbamazepine (CBZ), ibuprofen (IBP) and estrogens (E1, E2 and EE2) were chosen as model compounds to evaluate the catalyst for the simultaneous removal of pharmaceuticals (For the chemical structures check Fig. S3). The experiments were performed at pH 3, with a catalyst concentration of 131 mg L^{-1} and a hydrogen peroxide concentration of 223 mg L^{-1}. The kinetic parameters were fitted to pseudo-first order model and plotted in Fig. S4.

According to the results, the most recalcitrant compound was CBZ. The resistance of carbamazepine to degradation by advanced oxidation processes was previously observed by other authors (Luo et al., 2020; Monteoliva-García et al., 2019), thus justifying its selection as a model compound. Correlation coefficient values were satisfactory for all compounds, reaching values above 0.97, concluding that the pseudo-first-order model accurately represents the system performance. The kinetic parameters, compound half-life, regression coefficient and electrical energy per order for each pollutant are compiled in Table 1.

The kinetic constant for the removal of CBZ agrees with the results reported by Ioffe et al. (2021) using a system with a composite of activated carbon and magnetite ($k_{CBZ} = 0.4\ h^{-1}$) and persulfate as oxidant. In their work, the ratio between the removal rates of BPA and CBZ was 9, supporting the recalcitrant character of this compound. On the other hand, Luo et al. (2020) reported a BPA degradation of 93% in 30 min

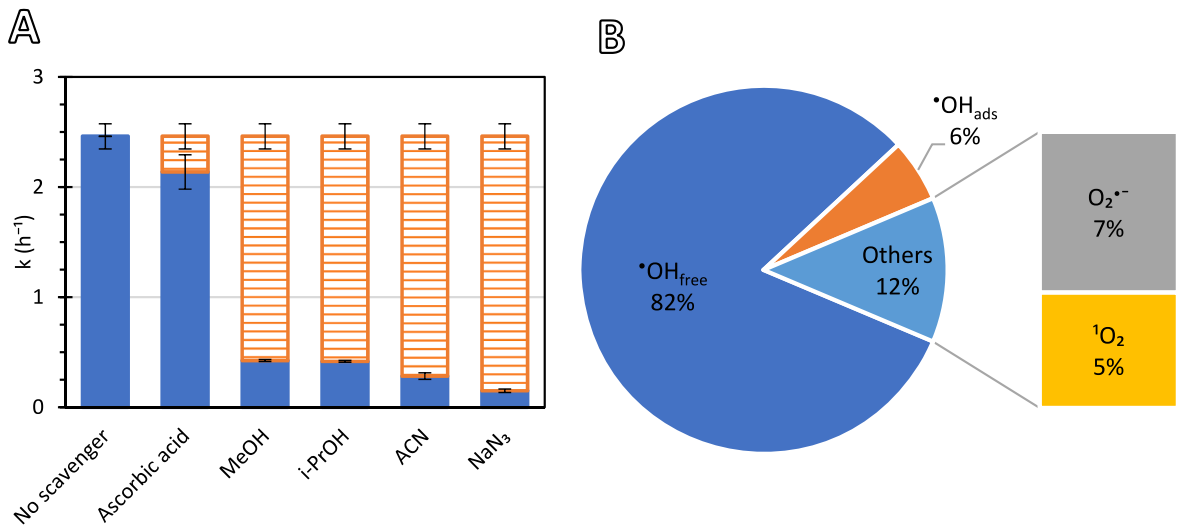

Fig. 3. (A) Reaction rates using different scavenging agents and (B) effect of quenching agents on PR degradation; [PR] = 10 mg L^{-1}, [Ascorbic acid] = 100 mg L^{-1}, [MeOH] = 1 g L^{-1},[i-PrOH] = 1 g L^{-1},[NaN_3] = 100 mg L^{-1}. Test with ACN was made using it as reaction solvent.

Table 1
Kinetic parameters for the removal of selected ECs under the optimum conditions.

Compound	k (h^{-1})	$t_{1/2}$ (h^{-1})	R^2	E_{Eo}(kWh m^{-3} $order^{-1}$)
CBZ	0.522 ± 0.089	1.33 ± 0.23	0.979	303.0
BPA	1.079 ± 0.111	0.64 ± 0.07	0.992	154.5
E1	1.611 ± 0.295	0.43 ± 0.08	0.976	103.5
E2	1.586 ± 0.235	0.44 ± 0.06	0.984	105.1
EE2	1.379 ± 0.164	0.50 ± 0.06	0.99	120.9

although the degradation of CBZ at the same time was 65%, using a heterogeneous system with MoS_2 and dissolved iron without irradiation. These values showed that the modification of nanoparticles by supporting them over SBA-15 to improve their recoverability is not affecting to the catalytic performance.

The catalyst showed excellent performance for the degradation of estrogens (E1, E2 and EE2), achieving significantly higher removal rates than those obtained for CBZ. There are reports in the literature showing similar degradation values for photo-Fenton systems (Baycan and Li Puma, 2018). These authors reported removal percentages around 80% of E1, E2 and EE2 after 1 h under UVA irradiation, reaching similar removal rates to those obtained in this study. However, in our case, the use of magnetic nanoparticles favors the recoverability and reuse of the catalysts, reducing the nanoparticle requirements. Although the kinetic values obtained were lower than those obtained using homogeneous photo-Fenton, the magnetic properties of the catalyst facilitate the separation after the reaction avoiding the release of iron species or the addition of stabilizing agents such as ethylenediamine-N,N′-disuccinic acid (EDDS) (Ahmed et al., 2022). In addition, all these tests were performed using a real wastewater matrix, so that the reduction of kinetics due to the presence of salts and organic substances was considered.

The influence of the photo-Fenton process on the inactivation of enteric bacteria was also evaluated. All these experiments were performed under optimal conditions and measuring an initial concentration of total coliforms of approximately 900 CFU mL^{-1} and 100 CFU mL^{-1} for *E. coli* (Table S1). These nanoparticles achieved complete inactivation of total coliforms and *E. coli* after 60 min of reaction, exposing the potentiality of this method for the joint removal of pharmaceuticals and microorganisms from wastewaters (Maniakova et al., 2021).

3.4. Reaction cycles

Catalyst recoverability is a critical factor for the potential scale-up of the process, as it minimizes catalyst consumption and improves the quality of the treated effluent. The efficacy of the separation process was verified by performing subsequent degradation cycles of the nanocomposite. At these experiments, the nanoparticles were separated from the effluent by the application of an external magnetic field to obtain the treated effluent and reusing the catalyst without further modification. The results of stability tests are shown in Fig. 4.

The catalytic activity of the nanoparticles showed no significant loss and remained constant after the experiments, ensuring excellent stability in subsequent cycles. Unlike the other pollutants, CBZ removal was observed to increase from 73% to values above 90% in the third cycle and continued to follow this trend thereafter. In this sense, the use of inert supports in heterogeneous catalysts based on Al_2O_3, SiO_2 or graphitic carbon nitride (g-C_3N_4) increases the performance of nanoparticles as their porous surfaces favor the contact between contaminants and catalysts (Liu et al., 2022; Wang et al., 2016), while showing an improvement in their stability in consecutive reaction cycles (González-Rodríguez et al., 2021).

The support of magnetite over SBA15 mesoporous silica provides to the pollutant higher reaction surfaces, leading to an increasing of the kinetics. Moreover, since the bare magnetite nanoparticles without supporting may suffer problems related to stability or agglomeration, the immobilization over a porous surface enhances their properties, as well as maintain high surface/volume ratios. Likewise, the surface of SBA15 act as support to facilitate the contact between the active catalysts and the target pollutants.

Leaching of iron species was determined by ICP on the treated effluent (Table 2). Although the maximum iron loss was reached after the third cycle with a concentration of 2.55 mg L^{-1}, the average iron leaching was 1.28 mg L^{-1}, which is a good indicator of the reusability of the nanoparticles. Considering the use of solid nanostructured catalysts, it was postulated that heterogeneous Fenton mechanisms are mainly responsible for the reduction of pollutants in this reaction system. The results of the iron species quantification after the reaction cycles using the magnetic separation indicated very low iron content, thus confirming that there was no contribution of homogeneous Fenton.

The degree of mineralization of the micropollutants after the treatment was quantified by the determination of the total organic carbon (TOC) content of samples before and after each cycle. TOC removal showed a high variability throughout the reaction cycles, with values

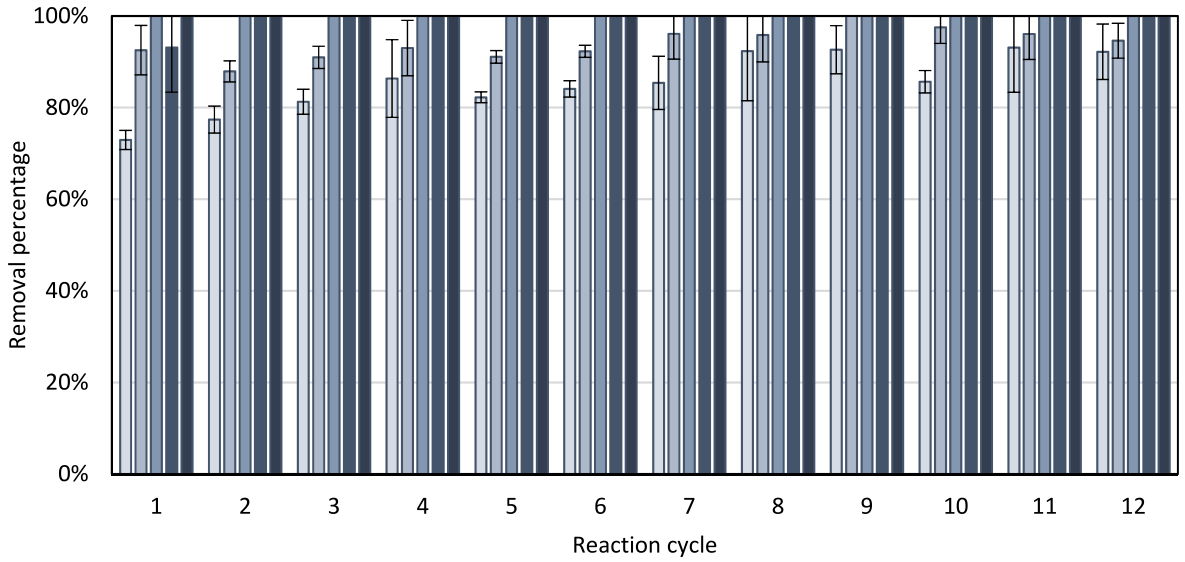

Fig. 4. Reaction cycles using real wastewater under magnetic separation, under the best operational conditions obtained by RSM analysis for the removal 300 μg L^{-1} of CBZ, BPA, E1, E2 and EE2 (lighter to dark) after 120 min of reaction.

Table 2
Iron content of effluents, total organic carbon (TOC) removal and toxicity measured before and after reaction cycles.

Cycle	[Fe] effluent (mg L^{-1})	TOC removal	Toxicity		
			$EC_{50,5}$	$EC_{50,15}$	$EC_{50,30}$
Real wastewater	n/a[1]	n/a	<LOD[2]	<LOD	<LOD
Initial value	n/a	n/a	28.1%	34.1%	36.4%
1	1.03 ± 0.02	21.1% ± 16.0%			
2	0.71 ± 0.01	11.2% ± 9.4%	31.7%	28.2%	44.7%
3	2.55 ± 0.06	17.8% ± 3.4%			
4	1.46 ± 0.03	6.7% ± 8.9%	17.4%	20.5%	42.3%
5	1.55 ± 0.08	6.1% ± 4.9%			
6	1.58 ± 0.01	18.9% ± 7.8%	18.2%	13.0%	17.7%
7	0.95 ± 0.04	15.4% ± 4.2%			
8	1.72 ± 0.02	21.9% ± 16.7%			
9	0.62 ± 0.02	15.8% ± 8.4%	19.0%	21.3%	74.3%
10	1.51 ± 0.08	6.0% ± 8.6%			
11	0.57 ± 0.01	23.0% ± 6.3%			
12	1.14 ± 0.01	17.6% ± 2.6%	18.6%	18.2%	27.7%
Average	1.28 ± 0.04	15.1% ± 9.2%	21.0% ± 6.0%	20.3% ± 5.5%	41.3% ± 21.5%

[1] n/a: not allowable; [2] LOD: limit of detection.

ranging from 6% to 23%, however no clear dependence between the removal cycle and TOC removal was detected, presenting an average of 15.1% ± 9.2% of the initial TOC removed. The values for TOC elimination in each of the cycles are also shown in Table 2. Since the mineralization of the target micropollutants was below 20% in most cycles, the characterization of the toxicity of effluents (using MicroTox assays with *Aliivibrio fischeri*) was considered to account for the potential generation of toxic degradation products. The toxicity assays showed that there was not a specific toxicity due to the presence of intermediates of reaction, since a considerable decrease of toxicity was not observed in the effluents of subsequent cycles compared to the initial toxicity values (see Table 2).

Other authors have studied reaction cycles considering several types of supported nanomaterials, mostly using non-magnetic catalysts. In this regard, Hernández-Oloño et al. (2021) analyzed the reusability of Fe/Al_2O_3 nanoparticles in five subsequent reaction cycles using dyes as model compounds, with similar degradation percentages throughout the experiments. The use of $MnZnFeO/g\text{-}C_3N_4$ as catalysts was studied by Saeed et al. (2021) in three reaction cycles also providing good nanoparticle stability, however, the use of non-magnetic heterogeneous catalyst by Xiang et al. (2020) showed a reduction in degradation percentages from complete removal to 57% in the fourth cycle. Therefore, the effective recoverability and reusability of these nanoparticles was demonstrated as the degradation rates were maintained in twelve subsequent reaction cycles without a reconditioning step in between.

3.5. Characterization of degradation by-products

Considering the low degree of mineralization of studied compounds, the characterization of degradation by-products was also evaluated to gain further insights on the degradation mechanisms of the micropollutants. Estrogens were considered as the most suitable compounds for the analysis of the formation of intermediate products since the parent compounds were completely removed from the water matrix. The formation of intermediates on the removal of E1, E2 and EE2 was studied to elucidate the degradation routes produced by Fenton-based abatement. Previously reported compounds appearing on unspecific oxidation of estrogens were collected from bibliographic sources to be detected by means of UHPLC-MS/MS. A complete list of the targeted compounds in the analysis is presented in Table S7 of the Supplementary Material.

Two types of intermediates were detected, based on the time in which appears in the reaction media, i.e., intermediates formed in the degradation of the parent compound and intermediates, formed in a

second step at reaction times higher than 10 min, generated in the subsequent degradation steps. The results of the detection of these intermediates in the degradation of estrone are shown in Fig. 5. The TP-290A was detected by Zhao et al. (2008) in the degradation of E2, and considering the similarity of the two hormones, is expected their formation also in E1 degradation. Moreover, the TP-276 was identified by Segura et al. (2013) as one of the main transformation product of estrone using ozonation. The authors reported the formation of another main transformation product identified as TP-318 that was not detected at this work. However, a secondary transformation compound (TP-160) reported by these authors was observed as part of fragmentation tree of TP-318, so probably the generation and degradation of this product occurred between the initial 15 min of the experiment.

Four degradation compounds formed in later stages of the oxidation route were detected, based on mass spectrometry analysis. The increase of mass in 16 u suggest that the three compounds designed as TP-286A/B/C are modifications of initial structure of estrone due to the addition of hydroxyl group to a cyclic carbon. This behavior was reported by other authors as Sornalingam et al. (2018) or Li and Zhang (2014) and related to a free radical addition of $^{\bullet}OH$ in aliphatic or aromatic ring (Zhao et al., 2008). The different retention times of transformation products with same elemental composition ($C_{18}H_{22}O_3$) is in line with the occurrence of nucleophilic attack in different carbons of the parent molecule. The presence of TP-290B was also detected, and as well as the previous case, the variation between the two compounds were the different retention times. The formation of dihydroxy products and quinone-like products stem from the hydroxylation of aromatic rings, while the formation of ketones and alcohols are related to the reaction of radicals with aliphatic rings. Moreover, the intermediate TP-290A was also isolated in the degradation pathway of E2 (Zhao et al., 2008). The transformation of ketone group into alcohol group in presence of $^{\bullet}O_2^-$ to form E2 from E1 was reported by Zhu et al. (2020) and it explains the similar degradation routes obtained for both compounds. The subsequent attack of $^{\bullet}OH$ and $HO_2^{\bullet}$ is reported to lead to the complete mineralization of these byproducts (Chhor et al., 2004).

In the case of E2, at the first stage of reaction the transformation products TP-160, TP-276 and TP-290A were detected, similarly to E1. The formation of TP-290B was also observed in the first measurement. As secondary transformation products, three different isomers of E1 were detected (with a retention time lower than the parent compound), probably caused by the similar structure of these two molecules. Another secondary product found was the TP-288, that is a modification of estrogen E2 with hydroxylation. The degradation of EE2 appears to follow a similar route, except for the formation of TP-344 at 60 min. This molecule was also reported by Sun et al. (2010) when analyzing the degradation of EE2 by photocatalysis. The formation of two carboxylic acids in the degradation of phenol-like structure is according to the results reported by Devi and Rajashekhar (2011) using photocatalysis-based reactions. The results of transformation products formed during the degradation of E2 and EE2 are shown in Fig. S4 and Tables S8–S10 of the Supplementary Material.

4. Conclusions

The effectiveness of Fe_3O_4@PAA/SBA-15 nanoparticles for the removal of a model dye and different types of pharmaceuticals was demonstrated, coupled to a reduction of energy requirements by using LED light instead of conventional UV sources, obtaining an E_{Eo} of 67.72 kW m^{-3} $order^{-1}$. Furthermore, the results obtained in twelve subsequent reaction cycles using the recovered nanoparticles showed the potential of the nanocomposite for recoverability using magnetic fields. In most cycles, removal rates above 90% for the target pollutants were achieved within 60 min, positioning the evaluated nanocomposite as a realistic candidate for implementation in tertiary wastewater treatments. Radical generation quantification concluded that the main contribution to the photo-Fenton process is based on free hydroxyl radicals, followed by adsorbed hydroxyl radicals, superoxide, and singlet oxygen. Response surface methodology was applied to optimize relevant operation variables, achieving a maximum kinetic constant of 2.6 h^{-1} for the degradation of ProcionRed®, as well as similar values in the degradation of carbamazepine, bisphenol A and estrogens. Although complete mineralization of these target compounds was not achieved, common transformation products were detected, demonstrating the feasibility of the process to achieve the complete degradation of contaminants. Among the pharmaceutical pollutants, carbamazepine was the most recalcitrant compound among the analyzed with a half-life of 1.33 h, since bisphenol A provided a half-life of 0.64 h and estrogens values were below 0.50 h.

These results pave the way for the use of magnetic supported catalysts as a viable and cost-effective alternative to conventional Fenton processes. Furthermore, the paramagnetic properties of the nanocatalysts allow for an easy separation of the effluent after treatment, thus reducing the operational costs associated with more complex separation steps.

Funding

This research was supported by HP-NANOBIO [PID2019-111163RB-I00] and MAGDEMON [PID2020-112626RB] projects, funded by MCIN/

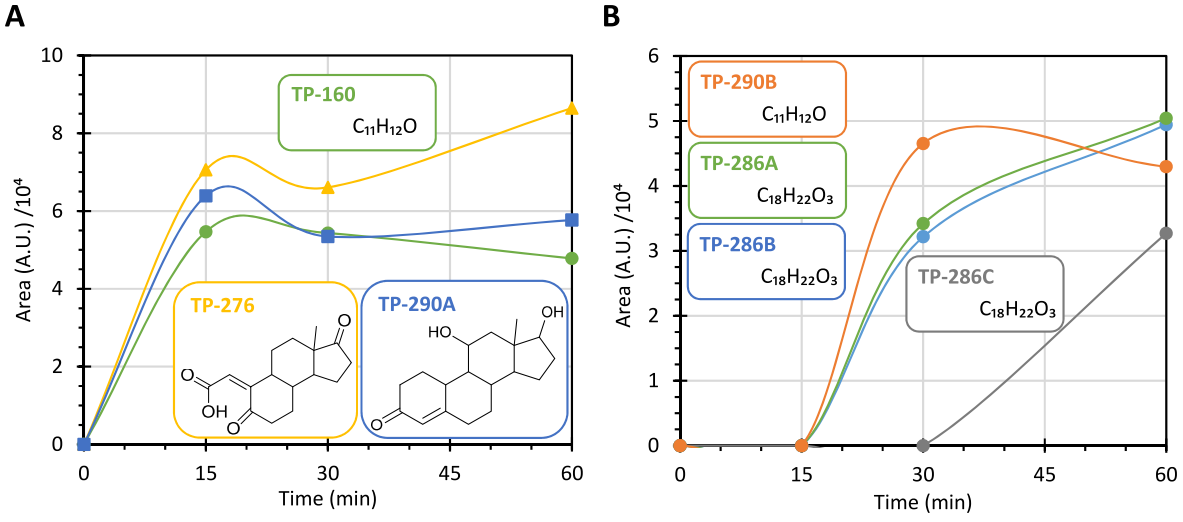

Fig. 5. Transformation products of estrone (E1) detected by UHPLC-MS/MS at (A) earlier and (B) later stages of reaction.

AEI/10.13039/501100011033 and SPOTLIGHT [PDC2021-121540-I00] project, funded by MCIN/AEI/10.13039/501100011033 and European Union NextGenerationEU/PRTR.

Declaration of competing interest

The authors declare that they have no known competing financial interests or personal relationships that could have appeared to influence the work reported in this paper.

Data availability

Data will be made available on request.

Acknowledgements

J.G.-R. thanks MCIN/AEI/10.13039/501100011033 for their FPU predoctoral fellowship [FPU19/00461] and J.J.C. thanks Xunta de Galicia for his postdoctoral fellowship [ED481B-2021/015]. The authors belong to the Galician Competitive Research Groups (GRC) ED431C-2021/16 and ED432C-2021/37, co-funded by FEDER (EU). Authors would like to thank the use of RIAIDT-USC analytical facilities (mass spectrometry and proteomics).

Appendix A. Supplementary data

Supplementary data to this article can be found online at https://doi.org/10.1016/j.jenvman.2023.119461.

References

Abd Manan, T.S.B., Khan, T., Sivapalan, S., Jusoh, H., Sapari, N., Sarwono, A., Ramli, R. M., Harimurti, S., Beddu, S., Sadon, S.N., Kamal, N.L.M., Malakahmad, A., 2019. Application of response surface methodology for the optimization of polycyclic aromatic hydrocarbons degradation from potable water using photo-Fenton oxidation process. Sci. Total Environ. 665, 196–212. https://doi.org/10.1016/j.scitotenv.2019.02.060.

Ahmed, Y., Zhong, J., Yuan, Z., Guo, J., 2022. Roles of reactive oxygen species in antibiotic resistant bacteria inactivation and micropollutant degradation in Fenton and photo-Fenton processes. J. Hazard Mater. 430, 128408 https://doi.org/10.1016/J.JHAZMAT.2022.128408.

Baycan, N., Li Puma, G., 2018. Nanostructured catalysts for photo-oxidation of endocrine disrupting chemicals. J. Photochem. Photobiol. Chem. 364, 274–281. https://doi.org/10.1016/J.JPHOTOCHEM.2018.05.010.

Chhor, K., Bocquet, J.F., Colbeau-Justin, C., 2004. Comparative studies of phenol and salicylic acid photocatalytic degradation: influence of adsorbed oxygen. Mater. Chem. Phys. 86, 123–131. https://doi.org/10.1016/j.matchemphys.2004.02.023.

Colilla, M., Balas, F., Manzano, M., Vallet-Regí, M., 2007. Novel method to enlarge the surface area of SBA-15. Chem. Mater. 19, 3099–3101. https://doi.org/10.1021/cm071032p.

Couto, C.F., Lange, L.C., Amaral, M.C.S., 2019. Occurrence, fate and removal of pharmaceutically active compounds (PhACs) in water and wastewater treatment plants—a review. J. Water Proc. Eng. 32, 100927 https://doi.org/10.1016/j.jwpe.2019.100927.

Craddock, H.A., Chattopadhyay, S., Rjoub, Y., Rosen, D., Greif, J., Lipchin, C., Mongodin, E.F., Sapkota, A.R., 2020. Antibiotic-resistant *Escherichia coli* and *Klebsiella spp.* in greywater reuse systems and pond water used for agricultural irrigation in the West Bank, Palestinian Territories. Environ. Res. 188 https://doi.org/10.1016/j.envres.2020.109777.

Da Cruz Severo, E., Dotto, G.L., Silvestri, S., Dos Santos Nunes, I., Da Silveira Salla, J., Martinez-De La Cruz, A., Da Boit Martinello, K., Foletto, E.L., 2020. Improved catalytic activity of EDTA–modified $BiFeO_3$ powders for remarkable degradation of procion red by heterogeneous photo–Fenton process. J. Environ. Chem. Eng. 8, 103853 https://doi.org/10.1016/J.JECE.2020.103853.

de Boer, S., González-Rodríguez, J., Conde, J.J., Moreira, M.T., 2022. Benchmarking tertiary water treatments for the removal of micropollutants and pathogens based on operational and sustainability criteria. J. Water Proc. Eng. 46, 102587 https://doi.org/10.1016/j.jwpe.2022.102587.

Deng, Y., Wei, J., Sun, Z., Zhao, D., 2013. Large-pore ordered mesoporous materials templated from non-Pluronic amphiphilic block copolymers. Chem. Soc. Rev. 42, 4054–4070. https://doi.org/10.1039/C2CS35426H.

Deng, Y., Zhao, R., 2015. Advanced oxidation processes (AOPs) in wastewater treatment. Curr Pollut Rep 1, 167–176. https://doi.org/10.1007/s40726-015-0015-z.

DeNicola, E., Aburizaiza, O.S., Siddique, A., Khwaja, H., Carpenter, D.O., 2015. Climate change and water scarcity: the case of Saudi Arabia. Ann Glob Health 81, 342–353. https://doi.org/10.1016/j.aogh.2015.08.005.

Devi, L.G., Rajashekhar, K.E., 2011. A kinetic model based on non-linear regression analysis is proposed for the degradation of phenol under UV/solar light using nitrogen doped TiO_2. J. Mol. Catal. Chem. 334, 65–76. https://doi.org/10.1016/j.molcata.2010.10.025.

Donadelli, J.A., Berardozzi, E., Carlos, L., García Einschlag, F.S., 2020. Continuous treatment of an azo dye based on a combined ZVI/photo-Fenton setup. Process modelling by response surface methodology. J. Water Proc. Eng. 37 https://doi.org/10.1016/j.jwpe.2020.101480.

Feng, M., Wang, Z., Dionysiou, D.D., Sharma, V.K., 2018. Metal-mediated oxidation of fluoroquinolone antibiotics in water: a review on kinetics, transformation products, and toxicity assessment. J. Hazard Mater. 344, 1136–1154. https://doi.org/10.1016/j.jhazmat.2017.08.067.

Ferreira, L.C., Fernandes, J.R., Peres, J.A., Tavares, P.B., Lucas, M.S., 2021. Wireless UV-A LEDs-driven AOP in the treatment of agro-industrial wastewaters. Environ. Res. 200, 111430 https://doi.org/10.1016/j.envres.2021.111430.

Gavrilescu, M., Demnerová, K., Aamand, J., Agathos, S., Fava, F., 2015. Emerging pollutants in the environment: present and future challenges in biomonitoring, ecological risks and bioremediation. N. Biotech. 32, 147–156. https://doi.org/10.1016/j.nbt.2014.01.001.

González-Rodríguez, J., Fernández, L., Vargas-Osorio, Z., Vázquez-Vázquez, C., Piñeiro, Y., Rivas, J., Feijoo, G., Moreira, M.T., 2021. Reusable Fe_3O_4/SBA15 nanocomposite as an efficient photo-fenton catalyst for the removal of sulfamethoxazole and orange II. Nanomaterials 11, 533. https://doi.org/10.3390/nano11020533.

Grassi, P., Drumm, F.C., Georgin, J., Franco, D.S.P., Foletto, E.L., Dotto, G.L., Jahn, S.L., 2020. Water treatment plant sludge as iron source to catalyze a heterogeneous photo-Fenton reaction. Environ. Technol. Innov. 17, 100544 https://doi.org/10.1016/J.ETI.2019.100544.

Gultekin, I., Ince, N.H., 2004. Degradation of reactive azo dyes by UV/H_2O_2: impact of radical scavengers. Journal of Environmental Science and Health, Part A 39, 1069–1081. https://doi.org/10.1081/ESE-120028414.

Hernández-Oloño, J.T., Infantes-Molina, A., Vargas-Hernández, D., Domínguez-Talamantes, D.G., Rodríguez-Castellón, E., Herrera-Urbina, J.R., Tánori-Córdova, J. C., 2021. A novel heterogeneous photo-Fenton Fe/Al_2O_3 catalyst for dye degradation. J. Photochem. Photobiol. Chem. 421, 113529 https://doi.org/10.1016/j.jphotochem.2021.113529.

Ioffe, M., Long, M., Radian, A., 2021. Systematic evaluation of activated carbon-Fe_3O_4 composites for removing and degrading emerging organic pollutants. Environ. Res. 198, 111187 https://doi.org/10.1016/J.ENVRES.2021.111187.

Kokate, S., Gupta, S., Kopuri, V.G., Prakash, H., 2022. Energy efficient photocatalytic activation of peroxymonosulfate by g-C_3N_4 under 400 nm LED irradiation for degradation of Acid Orange 7. Chemosphere 287, 132099. https://doi.org/10.1016/j.chemosphere.2021.132099.

Li, Y., Zhang, A., 2014. Removal of steroid estrogens from waste activated sludge using Fenton oxidation: influencing factors and degradation intermediates. Chemosphere 105, 24–30. https://doi.org/10.1016/j.chemosphere.2013.10.043.

Liu, Y., Wang, X., Sun, Q., Yuan, M., Sun, Z., Xia, S., Zhao, J., 2022. Enhanced visible light photo-Fenton-like degradation of tetracyclines by expanded perlite supported $FeMo_3O_x$/g-C_3N_4 floating Z-scheme catalyst. J. Hazard Mater. 424, 127387 https://doi.org/10.1016/j.jhazmat.2021.127387.

Lu, Y., Song, S., Wang, R., Liu, Z., Meng, J., Sweetman, A.J., Jenkins, A., Ferrier, R.C., Li, H., Luo, W., Wang, T., 2015. Impacts of soil and water pollution on food safety and health risks in China. Environ. Int. 77, 5–15. https://doi.org/10.1016/j.envint.2014.12.010.

Luo, H., Cheng, Y., Zeng, Y., Luo, K., Pan, X., 2020. Enhanced decomposition of H_2O_2 by molybdenum disulfide in a Fenton-like process for abatement of organic micropollutants. Sci. Total Environ. 732, 139335 https://doi.org/10.1016/J.SCITOTENV.2020.139335.

Lv, X., Huang, W., Ding, X., He, J., Huang, Q., Tan, J., Cheng, H., Feng, J., Li, L., 2020. Preparation and photocatalytic activity of Fe_3O_4@SiO_2@ZnO:La. J. Rare Earths. https://doi.org/10.1016/j.jre.2020.04.007.

Lyngsie, G., Krumina, L., Tunlid, A., Persson, P., 2018. Generation of hydroxyl radicals from reactions between a dimethoxyhydroquinone and iron oxide nanoparticles. Sci. Rep. 8, 10834 https://doi.org/10.1038/s41598-018-29075-5.

Maniakova, G., Salmerón, I., Polo-López, M.I., Oller, I., Rizzo, L., Malato, S., 2021. Simultaneous removal of contaminants of emerging concern and pathogens from urban wastewater by homogeneous solar driven advanced oxidation processes. Sci. Total Environ. 766, 144320 https://doi.org/10.1016/J.SCITOTENV.2020.144320.

Martínez-Alcalá, I., Guillén-Navarro, J.M., Lahora, A., 2020. Occurrence and fate of pharmaceuticals in a wastewater treatment plant from southeast of Spain and risk assessment. J. Environ. Manag. https://doi.org/10.1016/j.jenvman.2020.111565.

Massart, R., 1981. Preparation of aqueous magnetic liquids in alkaline and acidic media. IEEE Trans. Magn. 17, 1247–1248. https://doi.org/10.1109/TMAG.1981.1061188.

Minella, M., Marchetti, G., De Laurentiis, E., Malandrino, M., Maurino, V., Minero, C., Vione, D., Hanna, K., 2014. Photo-Fenton oxidation of phenol with magnetite as iron source. Appl. Catal., B 154–155, 102–109. https://doi.org/10.1016/j.apcatb.2014.02.006.

Mirzaei, A., Chen, Z., Haghighat, F., Yerushalmi, L., 2017. Removal of pharmaceuticals from water by homo/heterogonous Fenton-type processes – a review. Chemosphere 174, 665–688. https://doi.org/10.1016/j.chemosphere.2017.02.019.

Monteoliva-García, A., Martín-Pascual, J., Muñío, M.M., Poyatos, J.M., 2019. Removal of carbamazepine, ciprofloxacin and ibuprofen in real urban wastewater by using light-driven advanced oxidation processes. Int. J. Environ. Sci. Technol. 16, 6005–6018. https://doi.org/10.1007/s13762-019-02365-9.

Müller, A.B., Avellán, T., Schanze, J., 2020. Risk and sustainability assessment framework for decision support in "water scarcity – water reuse" situations. J. Hydrol. (Amst.) 591. https://doi.org/10.1016/j.jhydrol.2020.125424.

Nadeem, N., Yaseen, M., Rehan, Z.A., Zahid, M., Shakoor, R.A., Jilani, A., Iqbal, J., Rasul, S., Shahid, I., 2022. Coal fly ash supported $CoFe_2O_4$ nanocomposites: synergetic Fenton-like and photocatalytic degradation of methylene blue. Environ. Res. 206, 112280 https://doi.org/10.1016/j.envres.2021.112280.

Pai, C.W., Leong, D., Chen, C.Y., Wang, G.S., 2020. Occurrences of pharmaceuticals and personal care products in the drinking water of Taiwan and their removal in conventional water treatment processes. Chemosphere 256, 127002. https://doi.org/10.1016/j.chemosphere.2020.127002.

Pisharody, L., Gopinath, A., Malhotra, M., Nidheesh, P.V., Kumar, M.S., 2022. Occurrence of organic micropollutants in municipal landfill leachate and its effective treatment by advanced oxidation processes. Chemosphere 287, 132216. https://doi.org/10.1016/j.chemosphere.2021.132216.

Proctor, K., Petrie, B., Lopardo, L., Muñoz, D.C., Rice, J., Barden, R., Arnot, T., Kasprzyk-Hordern, B., 2021. Micropollutant fluxes in urban environment – a catchment perspective. J. Hazard Mater. 401 https://doi.org/10.1016/j.jhazmat.2020.123745.

Rambu, A.P., Nadejde, C., Schneider, R.J., Neamtu, M., 2018. Thin films containing oxalate-capped iron oxide nanomaterials deposited on glass substrate for fast Fenton degradation of some micropollutants. Environ. Sci. Pollut. Control Ser. 25, 6802–6813. https://doi.org/10.1007/s11356-017-1022-y.

Rodrigues, C.S.D., Madeira, L.M., Boaventura, R.A.R., 2009. Optimization of the azo dye Procion Red H-EXL degradation by Fenton's reagent using experimental design. J. Hazard Mater. 164, 987–994. https://doi.org/10.1016/j.jhazmat.2008.08.109.

Sadegh, F., Politakos, N., de San Roman, E.G., Sanz, O., Modarresi-Alam, A.R., Tomovska, R., 2021. Toward enhanced catalytic activity of magnetic nanoparticles integrated into 3D reduced graphene oxide for heterogeneous Fenton organic dye degradation. Sci. Rep. 11, 1–16. https://doi.org/10.1038/s41598-021-97712-7.

Saeed, H., Nadeem, N., Zahid, M., Yaseen, M., Noreen, S., Jilani, A., Shahid, I., 2021. Mixed metal ferrite ($Mn_{0.6}Zn_{0.4}Fe_2O_4$) intercalated g-C_3N_4 nanocomposite: efficient sunlight driven photocatalyst for methylene blue degradation. Nanotechnology 32, 505714. https://doi.org/10.1088/1361-6528/ac2847.

Segura, P.A., Kaplan, P., Yargeau, V., 2013. Identification and structural elucidation of ozonation transformation products of estrone. Chem. Cent. J. 7, 1–11. https://doi.org/10.1186/1752-153X-7-74.

Sharma, V.K., 2012. Oxidation of Amino Acids, Peptides, and Proteins. John Wiley & Sons, Inc., Hoboken, NJ, USA https://doi.org/10.1002/9781118482469.

Smith, A.F., Nicoll, W.D., 1955. Stability of dilute alkaline solutions of hydrogen peroxide. Ind. Eng. Chem. 47, 2548–2554.

So, C.M., Cheng, M.Y., Yu, J.C., Wong, P.K., 2002. Degradation of azo dye Procion Red MX-5B by photocatalytic oxidation. Chemosphere 46, 905–912. https://doi.org/10.1016/S0045-6535(01)00153-9.

Sornalingam, K., McDonagh, A., Zhou, J.L., Johir, M.A.H., Ahmed, M.B., 2018. Photocatalysis of estrone in water and wastewater: comparison between Au-TiO_2 nanocomposite and TiO_2, and degradation by-products. Sci. Total Environ. 610, 521–530. https://doi.org/10.1016/j.scitotenv.2017.08.097. –611.

Sun, W., Li, S., Mai, J., Ni, J., 2010. Initial photocatalytic degradation intermediates/pathways of 17α-ethynylestradiol: effect of pH and methanol. Chemosphere 81, 92–99. https://doi.org/10.1016/j.chemosphere.2010.06.051.

Tufail, A., Price, W.E., Mohseni, M., Pramanik, B.K., Hai, F.I., 2020. A critical review of advanced oxidation processes for emerging trace organic contaminant degradation: mechanisms, factors, degradation products, and effluent toxicity. J. Water Proc. Eng. https://doi.org/10.1016/j.jwpe.2020.101778.

United Nations, 2015. Transforming Our World: the 2030 Agenda for Sustainable Development. United Nations.

Vanderford, B.J., Pearson, R.A., Rexing, D.J., Snyder, S.A., 2003. Analysis of endocrine disruptors, pharmaceuticals, and personal care products in water using liquid chromatography/tandem mass spectrometry. Anal. Chem. 75, 6265–6274. https://doi.org/10.1021/ac034210g.

Vargas-Osorio, Z., González-Gómez, M.A., Piñeiro, Y., Vázquez-Vázquez, C., Rodríguez-Abreu, C., López-Quintela, M.A., Rivas, J., 2017. Novel synthetic routes of large-pore magnetic mesoporous nanocomposites (SBA-15/Fe_3O_4) as potential multifunctional theranostic nanodevices. J. Mater. Chem. B 5, 9395–9404. https://doi.org/10.1039/c7tb01963g.

Wang, N., Zheng, T., Zhang, G., Wang, P., 2016. A review on Fenton-like processes for organic wastewater treatment. J. Environ. Chem. Eng. 4, 762–787. https://doi.org/10.1016/j.jece.2015.12.016.

Xiang, H., Ren, G., Yang, X., Xu, D., Zhang, Z., Wang, X., 2020. A low-cost solvent-free method to synthesize α-Fe_2O_3 nanoparticles with applications to degrade methyl orange in photo-fenton system. Ecotoxicol. Environ. Saf. 200, 110744 https://doi.org/10.1016/j.ecoenv.2020.110744.

Zhao, Y., Hu, J., Jin, W., 2008. Transformation of oxidation products and reduction of estrogenic activity of 17β-estradiol by a heterogeneous photo-Fenton reaction. Environ. Sci. Technol. 42, 5277–5284. https://doi.org/10.1021/es703253q.

Zhu, N., Li, C., Bu, L., Tang, C., Wang, S., Duan, P., Yao, L., Tang, J., Dionysiou, D.D., Wu, Y., 2020. Bismuth impregnated biochar for efficient estrone degradation: the synergistic effect between biochar and Bi/Bi_2O_3 for a high photocatalytic performance. J. Hazard Mater. 384, 121258 https://doi.org/10.1016/j.jhazmat.2019.121258.